CrystEngComm

PAPER

View Article Online
View Journal | View Issue

Cite this: *CrystEngComm*, 2014, **16**, 6635

Metal–organic frameworks with improved moisture stability based on a phosphonate monoester: effect of auxiliary N-donor ligands on framework dimensionality†

Jian-Wei Zhang,[ab] Cui-Cui Zhao,[a] Yin-Ping Zhao,[a] Hai-Qun Xu,[b] Zi-Yi Du*[ac] and Hai-Long Jiang*[bc]

Received 29th March 2014,
Accepted 19th April 2014

DOI: 10.1039/c4ce00655k

www.rsc.org/crystengcomm

A series of metal–organic frameworks (MOFs) based on a phosphonate monoester ligand, with structures featuring 1D chains, 2D layers or double layers, and 3D networks, have been successfully obtained in the presence of auxiliary N-donor ligands. The phosphonate monoester, behaving as a carboxylate linker, bridges metal ions, while the auxiliary N-donor ligands play a crucial role in both the structural diversity and the dimensionality variation of the resultant MOFs. Remarkably, the hydrophobic ethyl groups present in the phosphonate monoester linker offer protection/shielding for the hydrolytically vulnerable M–O bonds, resulting in the MOFs being highly moisture stable, as expected. The porous MOFs with 3D networks exhibited CO_2 adsorption and strong fluorescence emission.

Introduction

During the last two decades, as a relatively new type of porous crystalline materials, metal–organic frameworks (MOFs), also called porous coordination polymers, have attracted widespread attention due to their modular assembly, structural diversity, chemical tailorability and tunability, as well as potential applications in many fields, such as gas sorption and separation, catalysis, sensing, drug delivery, and so on.[1–5] In comparison with traditional porous materials, such as zeolites, activated carbon and mesoporous silica, it is fair to say that MOFs have many advantages, especially their crystallinity, tunability and modular nature, which allow MOF pore sizes ranging from ultra-microporous to mesoporous (0–4 nm or even larger). Thus, it is considered that MOFs with wide ranges of pore sizes bridge the gap between mesoporous silica with large pores and zeolites with very small pores.[3c] However, most previously reported MOFs are moisture sensitive, which has been recognized as an imperative issue for their practical applications. For example, as a classical and representative MOF, MOF-5 has been intensively studied for different ends, however the Zn_4O clusters are readily hydrolyzed upon exposure to water vapor, giving rise to collapse of the porous structure and/or phase change.[6] So far, several types of stable MOFs have been reported, such as zeolitic imidazolate frameworks (ZIFs), the MIL series, the UiO series, pyrazolates and triazolates, *etc.*,[7,8] which have been intensively studied for functional applications. Considering that the moisture sensitivity of MOFs could be caused by the weak metal–carboxylic oxygen bonds that are readily attacked by water molecules, we and others have recently developed a series of MOFs with very high chemical stability, based on the combination of a "hard acid", zirconium(IV), and a "hard base", carboxylate anions.[9,10]

To continue this research on targeting MOFs with enhanced moisture stability, we are interested in MOFs linked by organic phosphonate monoesters. Although phosphonic acid has been widely employed as an organic linker in the synthesis of metal phosphonates,[11] organic phosphonate monoesters are an underexplored class of ligands.[12] Recently, the bidentate oxygen donor ligation by phosphonate monoesters has been reported to be similar to the coordination mode of carboxylate anions.[12c–e] The self-assembly process of the phosphonate monoester with metal ions proceeds steadily to yield single crystals with suitable sizes. Moreover, it has been reported that moisture resistant MOFs can be obtained by post-synthetically grafting alkyl groups onto the organic linkers.[13] Therefore, the hydrophobic

[a] *College of Chemistry and Chemical Engineering, Gannan Normal University, Ganzhou 341000, PR China. E-mail: ziyidu@gmail.com*
[b] *Hefei National Laboratory for Physical Sciences at the Microscale, Department of Chemistry, University of Science and Technology of China, Hefei, Anhui 230026, PR China. E-mail: jianglab@ustc.edu.cn; Fax: +86 551 63607861*
[c] *State Key Laboratory of Structural Chemistry, Fujian Institute of Research on the Structure of Matter, Chinese Academy of Sciences, Fuzhou, Fujian 350002, PR China*

† Electronic supplementary information (ESI) available: X-ray crystallographic files (CCDC 978185–978192) for ligands and compounds **1**–**6** in CIF format, syntheses of organic ligands, and additional figures. For ESI and crystallographic data in CIF or other electronic format see DOI: 10.1039/c4ce00655k

alkyl group (–R) tethered on the ligand might function as a steric shield to protect the hydrolytically vulnerable M–O bonds and thus enhance the moisture stability of the resultant MOFs. Bearing this in mind, 4,4′-biphenyldiphosphonate bis(monoethyl ester) (H_2BPDP) was isolated, followed by assembly with an auxiliary N-donor ligand, bis(imidazol-1-yl)methane (BIM) or 1,3,5-tri(1H-imidazol-1-yl)benzene (TIB) to afford a series of MOFs: [Cd(BPDP)(BIM)(H_2O)$_2$] (**1**), [Cd(BPDP)(BIM)]·7H_2O (**2**), [Co(BPDP)(TIB)(H_2O)]·7H_2O (**3**), and [M(BPDP)(TIB)(H_2O)$_2$]·6H_2O (M = Cd for **4**, Co for **5**, and Cu for **6**), featuring 1D chains, a double layered structure, a layered structure, and 3D isomorphous frameworks, respectively. It is very interesting that coordination between the BPDP ligand and metal ions gives 1D chains for all MOFs, while the introduction of an auxiliary N-donor ligand extends the 1D chain to different framework dimensionalities. Remarkably, these MOFs based on a phosphonate monoester linker with ethyl group protection are highly moisture stable, as expected, and compounds **4** and **6** are capable of CO_2 adsorption, exhibiting permanent porosity upon solvent removal. The Cd-based MOFs have also shown strong fluorescence emissions assigned to intraligand transitions.

Experimental section

Materials and general methods

All solvents and reagents for syntheses were commercially available and used as received, except for organic ligands, which were synthesized using published procedures with modifications (see ESI†).[14] The FT-IR spectra were recorded on a Perkin-Elmer Spectrum 2000 FT-IR spectrometer using KBr pellets in the range of 4000–400 cm^{-1}. Thermogravimetric analyses (TGA) were carried out on a Shimadzu DTG-60H thermogravimetric-differential thermal analyzer at a ramp rate of 10 °C min^{-1} under nitrogen. Powder X-ray diffraction (XRD) patterns were obtained on a Japan Rigaku SmartLab™ rotation anode X-ray diffractometer or a Holland X'Pert PRO fixed anode X-ray diffractometer equipped with graphite monochromatized Cu Kα radiation (λ = 1.54178 Å). Solid state emission spectra were recorded using a Perkin-Elmer LS55 luminescence spectrophotometer under the same measurement conditions. The CO_2 adsorption/desorption isotherms were obtained using a Micrometritics ASAP 2020 system, and the sorption temperatures were controlled using a dry ice/acetone bath. Compound **4** was dried under a dynamic vacuum at 120 °C for 24 h. Before the measurements, the sample was dried again by using the "outgas" function of the surface area analyzer for 6 h at 120 °C. Compound **6** was subjected to solvent exchange (by soaking in methanol for over 1 day) and then treated using the same process as that used for compound **4** prior to the adsorption/desorption measurements.

Preparation of compounds 1–6

Preparation of [Cd(BPDP)(BIM)(H_2O)$_2$] (1). A mixture of H_2BPDP (74 mg, 0.2 mmol) and BIM (30 mg, 0.2 mmol) in 4 mL distilled water was introduced dropwise into a solution of Cd(CH_3COO)$_2$·2H_2O (53 mg, 0.2 mmol) in 4 mL distilled water under vigorous stirring. The resultant solution was filtered to give a filtrate. The filtrate was heated and spontaneously volatilized at ~80 °C for about 2 hours in a beaker to afford colorless plate-shaped single crystals of compound **1**. The measured XRD pattern was in good agreement with the one simulated from the crystal structure data. IR data (KBr, cm^{-1}): 3124 (m), 2974 (m), 1500 (m), 1400 (m), 1283 (m), 1238 (m), 1197 (s), 1143 (m), 1041 (s), 936 (m), 828 (m), 766 (m), 650 (m), 593 (m), 544 (m), 482 (m).

Preparation of [Cd(BPDP)(BIM)]·7H_2O (2). A mixture of Cd(NO_3)$_2$·4H_2O (31 mg, 0.1 mmol) and BIM (15 mg, 0.1 mmol) in 2 mL ethanol was introduced dropwise into a solution of H_2BPDP (55 mg, 0.15 mmol) in 4 mL hot ethanol during vigorous stirring and heating. This was followed by filtration. The filtrate was heated to 65 °C in a 20 mL vial for 1 day to yield colorless rod-shaped crystals of **2**. A pure phase of compound **2** has not been obtained, although much effort was exerted.

Preparation of [Co(BPDP)(TIB)(H_2O)]·7H_2O (3). A mixture of Co(CH_3COO)$_2$·4H_2O (25 mg, 0.1 mmol) and TIB (28 mg, 0.1 mmol) in a mixture of 1 mL ethanol and 1 mL distilled water was introduced dropwise into a solution of H_2BPDP (55 mg, 0.15 mmol) in 4 mL hot ethanol during vigorous stirring and heating. This was followed by filtration. The filtrate was heated to 65 °C in a 20 mL vial for 1 day to yield pink plate-shaped crystals of **3**. The measured XRD pattern was in good agreement with the one simulated from the crystal structure data. IR data (KBr, cm^{-1}): 3252 (m), 3113 (m), 1619 (m), 1561 (m), 1506 (vs), 1389 (m), 1309 (w), 1278 (m), 1143 (w), 1076 (m), 1014 (m), 931 (w), 874 (m), 812 (w), 757 (m), 676 (w), 638 (m).

Preparation of [M(BPDP)(TIB)(H_2O)$_2$]·6H_2O (M = Cd for 4, and Co for 5). The two compounds were prepared using a similar procedure to that used for **3**, except that Co(CH_3COO)$_2$·4H_2O was replaced by Cd(NO_3)$_2$·4H_2O for **4** and Co(NO_3)$_2$·6H_2O for **5**. Colorless and pink block-shaped crystals of **4** and **5**, respectively, were obtained. The measured XRD pattern of compound **4** was in good agreement with the one simulated from the crystal structure data, while a pure phase of compound **5** has not been obtained. IR data for **4** (KBr, cm^{-1}): 3376 (m), 3129 (m), 1622 (m), 1513 (m), 1381 (s), 1343 (m), 1177 (s), 1045 (vs), 937 (m), 826 (m), 759 (s), 646 (w), 586 (m), 525 (s), 462 (m).

Preparation of [Cu(BPDP)(TIB)(H_2O)$_2$]·6H_2O (6). A 4 mL aqueous solution (~75 °C) of Cu(NO_3)$_2$·3H_2O (93 mg, 0.2 mmol) was added dropwise to a mixture of H_2BPDP (93 mg, 0.25 mmol) and TIB (55 mg, 0.2 mmol) in 4 mL distilled water (~75 °C). The resultant solution was filtered to give a filtrate, which was heated and spontaneously volatilized at ~75 °C for about 2 hours in a beaker to yield green block-shaped crystals of **6**. The measured XRD pattern was in good agreement with the one simulated from the crystal structure data. IR data (KBr, cm^{-1}): 3122 (m), 2974 (w), 1618 (m), 1507 (s), 1292 (m), 1248 (m), 1179 (s), 1136 (w), 1046 (vs), 934 (s), 827 (m), 757 (m), 594 (m), 518 (m).

X-ray crystallography

Single crystal X-ray data collections for the organic ligands and all coordination compounds were performed on a Smart ApexII CCD diffractometer equipped with graphite monochromated Mo Kα radiation (λ = 0.71073 Å). Intensity data for all compounds were collected at 296 K. The data sets were corrected for Lorentz and polarization factors, as well as for absorption, using the SADABS program.[15] All structures were solved by direct methods and refined by full-matrix least-squares fitting on F^2 using SHELX-97.[16] C-bound H atoms were generated geometrically, while O-bound H atoms were located in the difference Fourier maps. All non-hydrogen atoms were refined with anisotropic thermal parameters, whereas all hydrogen atoms were refined isotropically. The hydrogen atoms in the water molecules in compounds **3–6** were not included in the refinements. The contributions of the disordered water molecules removed by the SQUEEZE process[17] are included in Table 1 for compounds **2**, **4**, **5** and **6**. The number of water molecules was estimated from the contribution of the electrons removed from the unit-cell contents, and detailed information can be found in the CIF files (see _platon_squeeze_details). For the structures of compounds **4–6**, the position disorder of the C(18) and N(4) atoms in one non-coordinated imidazole group of the TIB ligand was refined anisotropically using the PART, EXYZ and EADP instructions of SHELXL. Crystallographic data and structural refinements are summarized in Table 1. Important bond lengths are listed in Table 2.

Results and discussion

Monoester and diester ligands

In each phosphonate group, there are three O atoms connected to the P atom: one O atom is bonded to the P center with a double bond, while the other two O atoms are in hydroxide or ester form, and are bonded to the P center with single bonds. If both oxygen atoms are esterified (ESI,† Fig. S1), it would be difficult to coordinate the phosphonate diester group to any metal cations. If one oxygen atom is esterified (ESI,† Fig. S2), the phosphonate monoester group might behave as a carboxylic acid group and coordinate to metal cations to afford MOFs. Therefore, the monoester was employed for the following MOF syntheses.

[Cd(BPDP)(BIM)(H_2O)$_2$] (1). Compound **1** crystallizes in the $P\bar{1}$ space group. It contains two crystallographically unique cadmium(II) ions, two independent bridging ligands (BPDP and BIM) and two aqua ligands in the asymmetric unit. The unique Cd(1) and Cd(2) cations are located at two independent inversion centers, and each is octahedrally coordinated by three pairs of symmetry-related donors, *i.e.*, two O atoms from two phosphinate ligands, two N atoms from two BIM ligands, and two aqua ligands (Fig. 1). The water O–Cd bond lengths (2.368(2) and 2.414(2) Å) are slightly longer than the PO_3 O–Cd bond lengths (2.261(2) to 2.323(2) Å), and all of the bond lengths are comparable to those in previously reported cadmium(II) MOFs.[4b,18]

The BPDP and BIM ligands both act as end-to-end bidentate bridging ligands (Fig. S3†), and the interconnection of the Cd(II) ions by the above two types of ligands forms a 1D double-chain (Fig. 2a), which features an asymmetric four-membered ring unit containing one BPDP, one BIM and two Cd(II) ions. Corner-sharing of these ring units at the Cd(II) inversion centers results in a unique double-chain running along the *b*-axis. The discrete double-chains in compound **1** are further assembled into a compact three-dimensional structure *via* van der Waals forces, and no lattice water molecules are present in the structure (Fig. 2b).

[Cd(BPDP)(BIM)]·7H_2O (2). When the cadmium(II) source $Cd(CH_3COO)_2{\cdot}2H_2O$ used in the synthesis of compound **1** was replaced by $Cd(NO_3)_2{\cdot}4H_2O$ in ethanol, compound **2**, which has a double layered structure and crystallizes in the *C*2/*m* space group, was obtained. There are one crystallographically independent cadmium(II) ion lying on a 2-fold axis, one unique BPDP ligand related by 2-fold symmetry, and two types of BIM ligands related by 2-fold and mirror symmetries in the asymmetric unit. The Cd(II) ion is coordinated in a pseudo-octahedral environment by four nitrogen atoms from four BIM ligands and two oxygen atoms from two BPDP ligands (Fig. 3). The Cd–O and Cd–N bond distances are in a narrow and normal range of 2.306(4)–2.320(4) Å. Similar to compound **1**, the BPDP ligand is bidentate and bridges two Cd(II) ions with two oxygen atoms from P–O single bonds to form a 1D chain. In contrast, each of the two unique BIM ligands bridges two Cd(II) ions with two nitrogen atoms to give a nanoribbon-like chain along the *a*-axis, with a ribbon width of 1.67 nm in the *b*-direction (ESI,† Fig. S4). The two kinds of chains are interconnected in different directions to construct a thick 2D double layer in the *ac*-plane, in which quadrangle-like rings are composed of four Cd(II) ions, two BPDP ligands and two BIM ligands (Fig. 4). The thickness of the double layer is about 16.7 Å, and the inter-double-layer distance is 14.5 Å. In this case, the different double layers almost stack together without interlayer openings (ESI,† Fig. S4c).

[Co(BPDP)(TIB)(H_2O)]·7H_2O (3). By replacing Cd(II) with Co(II) and BIM with TIB, compound **3**, which crystallizes in the $P2_1/c$ space group with similar 2D sheets, was successfully obtained. As shown in Fig. 5, the asymmetric unit of **3** consists of one Co(II) center, one BPDP, one TIB and one aqua ligand, as well as seven lattice water molecules. The Co(II) ion is six-coordinated by three nitrogen atoms from three TIB ligands and two oxygen atoms from two BPDP ligands, as well as an aqua ligand. Similar to compound **1**, the water O–Co bond distance of 2.215(3) Å is slightly longer than the phosphonate O–Co bond distances and the TIB N–Co bond distances, which range from 2.065(3) to 2.128(4) Å, and are comparable to those in previously reported cobalt(II) MOFs.[19] Each of the two oxygen atoms with P–O single bonds in the BPDP ligand connects to one Co(II) ion to form a 1D wave-like chain, and the depth of the "wave" is slightly less than in compound **1**. Each nitrogen atom of the TIB ligand is bonded to one Co(II) cation to provide a 2D graphene-like layer in the *ab*-plane with large 6-membered rings, which are formed

Table 1 Crystallographic parameters from single crystal X-ray diffraction for the ligands and compounds **1–6**

Complexes	Phosphonate monoester	Phosphonate diester	**1**	**2**	**3**	**4**	**5**	**6**
Formula	$C_{18}H_{24}O_6P_2$	$C_{22}H_{32}O_6P_2$	$C_{25}H_{34}N_4O_8P_2Cd$	$C_{32}H_{52}O_{13}N_8P_2Cd$	$C_{33}H_{50}O_{14}N_6P_2Co$	$C_{33}H_{50}CdN_6O_{14}P_2$	$C_{33}H_{50}CoN_6O_{14}P_2$	$C_{33}H_{50}CuN_6O_{14}P_2$
Fw	398.31	454.42	692.90	931.16	875.67	929.13	875.66	880.27
Space group	$P\bar{1}$	$P2_1/c$	$P\bar{1}$	$C2/m$	$P2_1/c$	$C2/c$	$C2/c$	$C2/c$
a (Å)	7.6515(2)	15.8384(8)	8.9485(4)	17.4704(16)	10.2738(2)	21.7570(3)	21.5310(4)	21.6074(6)
b (Å)	8.0147(2)	8.4589(5)	13.0362(6)	28.935(2)	20.8895(5)	14.2474(2)	14.1050(2)	14.0197(4)
c (Å)	9.3307(2)	17.7369(11)	13.0950(6)	8.6998(7)	19.9247(5)	14.6058(2)	14.5410(2)	14.4710(4)
α (deg)	71.162(2)	90	82.8370(10)	90	90	90	90	90
β (deg)	67.620(2)	96.493(2)	71.0060(10)	113.244(2)	97.822(2)	118.1600(10)	117.4320(10)	117.832(2)
γ (deg)	84.036(2)	90	87.4860(10)	90	90	90	90	90
V (Å^3)	500.64(2)	2361.1(2)	1433.14(11)	4040.8(6)	4236.34(17)	3991.61(10)	3919.48(11)	3876.58(19)
Z	1	4	2	4	4	4	4	4
$d_{calcd.}$ (g cm^{-3})	1.321	1.278	1.606	1.531	1.373	1.546	1.484	1.508
μ (mm^{-1})	0.247	0.218	0.928	0.691	0.549	0.700	0.593	0.721
F(000)	210	968	708	1928	1836	1920	1836	1844
Reflections collected	4320	11 617	11 557	16 813	29 020	16 614	16 275	14 321
Independent reflections	2254	4634	5563	4064	8332	3918	3847	3807
Observed data [$I > 2\sigma(I)$]	1431	2339	4817	2728	4923	3047	2725	2005
Data/restraints/parameters	2254/0/118	4634/0/271	5563/9/376	4064/2/225	8332/3/505	3918/1/229	3847/1/229	3807/1/229
GOF on F^2	1.042	1.000	1.035	1.008	1.019	1.049	1.062	0.995
R_1,[a] wR_2[b] [$I > 2\sigma(I)$]	0.0518, 0.1208	0.0578, 0.1142	0.0272, 0.0709	0.0533, 0.1245	0.0670, 0.1660	0.0376, 0.1003	0.0532, 0.1408	0.0640, 0.1284
R_1,[a] wR_2[b] (all data)	0.0854, 0.1383	0.1295, 0.1422	0.0326, 0.0747	0.0813, 0.1369	0.1234, 0.1972	0.0497, 0.1051	0.0738, 0.1500	0.1212, 0.1452

[a] $R_1 = \sum||F_o| - |F_c||/\sum|F_o|$. [b] $wR_2 = \{\sum w[(F_o)^2 - (F_c)^2]^2/\sum w[(F_o)^2]^2\}^{1/2}$.

Table 2 Selected bond lengths (Å) for compounds 1–6[a]

1			
Cd(1)–O(1)	2.323(2)	Cd(1)–N(1)	2.324(2)
Cd(1)–O(1W)	2.368(2)	Cd(2)–O(5)	2.261(2)
Cd(2)–N(2)	2.262(2)	Cd(2)–O(2W)	2.414(2)
2			
Cd(1)–N(1)	2.306(4)	Cd(1)–O(1)	2.313(3)
Cd(1)–N(3)	2.320(4)		
3			
Co(1)–O(2)	2.065(3)	Co(1)–O(4)#1	2.079(3)
Co(1)–N(4)#2	2.110(4)	Co(1)–N(6)#3	2.115(4)
Co(1)–N(2)	2.130(4)	Co(1)–O(1W)	2.215(3)
4			
Cd(1)–N(2)#1	2.248(2)	Cd(1)–N(2)	2.248(2)
Cd(1)–O(1W)	2.354(2)	Cd(1)–O(1)	2.362(2)
5			
Co(1)–N(2)#1	2.105(3)	Co(1)–N(2)	2.105(3)
Co(1)–O(1W)	2.138(2)	Co(1)–O(1)	2.177(2)
6			
Cu(1)–N(2)#1	1.999(3)	Cu(1)–N(2)	1.999(3)
Cu(1)–O(1W)	2.050(3)	Cu(1)–O(1)	2.402(3)

[a] Symmetry codes: #1, $-x$, $y-1/2$, $-z+3/2$; #2, $-x+1$, $y+1/2$, $-z+3/2$; #3, $x-1$, y, z.

by three Co(II) ions and three TIB ligands (ESI,† Fig. S5). As a result, the Co–BPDP chains are grafted onto the Co–TIB layer by N–Co–O connectors, resulting in a layer that is not only slightly thicker, but also more "solid" (Fig. 6; ESI,† Fig. S5c). The interlayer distance in the *c*-axis direction is about 10 Å. From a topological perspective, the BPDP ligand can be viewed as a metal linker, while the Co(II) center and the TIB ligand can be defined as 5- and 3-connected nodes, respectively, and the interconnection of the two kinds of nodes in a 1 : 1 ratio gives a two-dimensional (3,5)-connected net (Fig. 6b).

$[M(BPDP)(TIB)(H_2O)_2]\cdot 7H_2O$ (M = Cd 4, Co 5, Cu 6). It is very interesting that using metal nitrate as the metal source in aqueous media seems to favour the formation of MOFs with 3D frameworks in our system. By replacing $Co(CH_3COO)_2\cdot 4H_2O$ with $Cd(NO_3)_2\cdot 4H_2O$ or $Co(NO_3)_2\cdot 6H_2O$

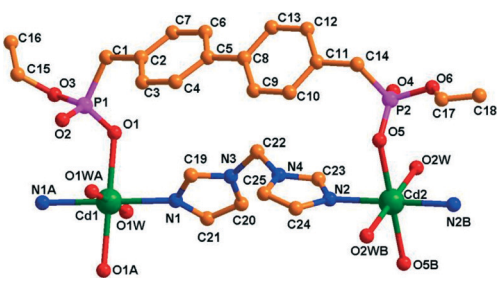

Fig. 1 Coordination environments of the cadmium(II) centers and the binding fashion of the BPDP and BIM ligands in compound **1**. Symmetry codes: A $-x$, $2-y$, $1-z$; B $2-x$, $1-y$, $1-z$.

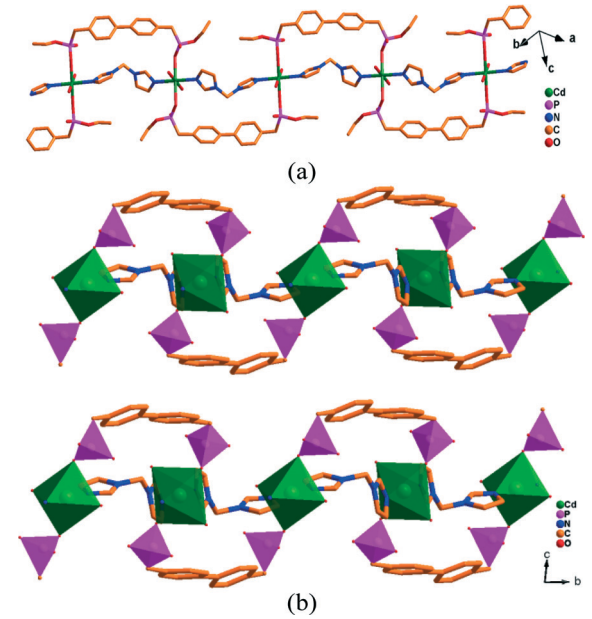

Fig. 2 (a) View of the 1D double-chain structure of **1**. (b) View of the overall structure of **1** down the *a*-axis. The CdO_2N_4 and PCO_3 polyhedra are shown in green and purple, respectively.

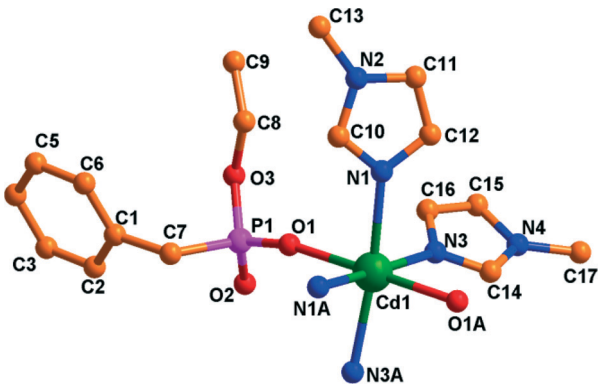

Fig. 3 Coordination environment of the cadmium(II) center and the binding fashion of the BPDP and BIM ligands in compound **2**. Symmetry code: A $1-x$, y, $2-z$.

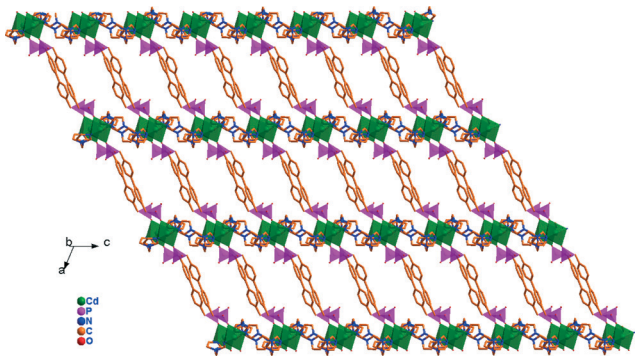

Fig. 4 View along the *b*-axis of the thick 2D double layer in the structure of compound **2**. The CdO_2N_4 and PCO_3 polyhedra are shown in green and purple, respectively.

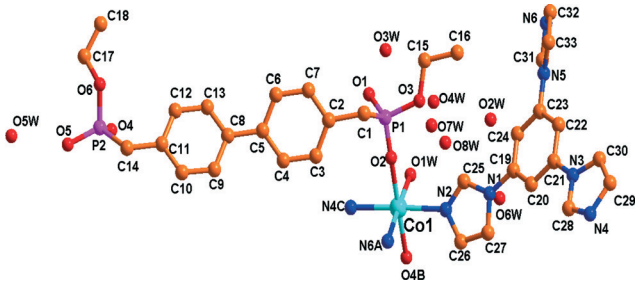

Fig. 5 Coordination environment of the cadmium(II) center and the binding fashion of the BPDP and TIB ligands in compound **3**. Symmetry code: A −1 + *x*, *y*, *z*; B −*x*, −0.5 + *y*, 1.5 − *z*; C 1 − *x*, 0.5 + *y*, 1.5 − *z*.

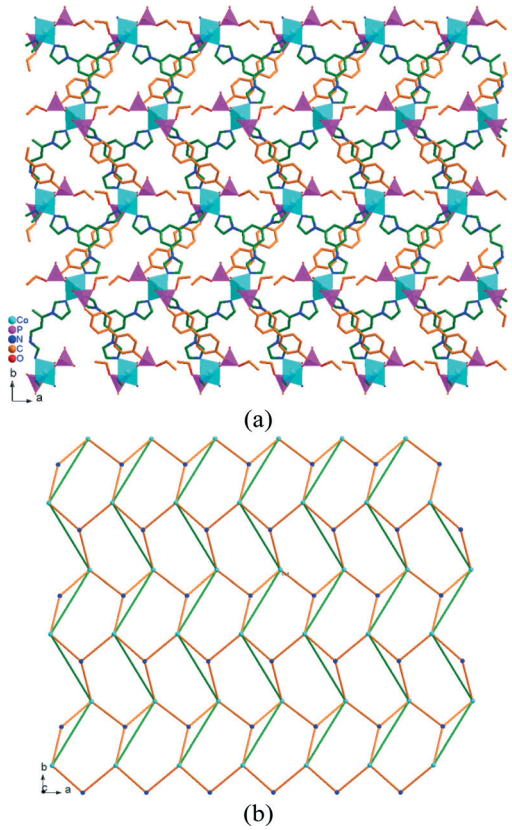

Fig. 6 (a) View of the 2D layered structure of compound **3** along the *c*-axis. The CoO_2N_4 and PCO_3 polyhedra are shown in cyan and purple, respectively. The C atoms in the TIB ligands are shown in green for clear recognition. (b) Topological view of the (3,5)-connected 2D layer, in which the TIB ligands and the Cd(II) ions are simplified as 3- and 5-connected nodes (blue and cyan atoms), respectively, and the BPDP ligands are simplified as green lines.

while keeping the other reaction parameters the same as those used for compound **3**, compounds **4** and **5** with 3D networks were obtained. Similarly, by employing $Cu(NO_3)_2{\cdot}3H_2O$ as the metal source and slightly changing the reaction conditions, compound **6** with a 3D structure was prepared. The unit-cell dimensions, volumes, related bond distances, and angles of compounds **4**–**6** are only slightly different. They are isomorphous and exhibit similar structures. Therefore, compound **4** will be discussed in detail as a representative. As shown in Fig. 7, there is one crystallographically unique Cd(II) ion with half-occupancy located at an inversion center, half a BPDP ligand located at another inversion center, and half a TIB ligand lying about a two-fold axis, as well as one aqua ligand, in the asymmetric unit. Almost the same as in compound **1**, the Cd(II) ion is pseudo-octahedrally coordinated by four oxygen atoms and two nitrogen atoms from two TIB ligands, in which two oxygen atoms are from two BPDP ligands and the other two oxygen atoms are from aqua ligands. The phosphonate and aqua O–Cd bond distances are similar, at 2.363(2) and 2.352(3) Å, respectively; the Cd–N bond distance is 2.246(3) Å, and all of the bond distances fall within normal ranges.[18] As described previously, the BPDP ligand acts as a bridge to connect two Cd(II) ions to give a wave-like chain. Strikingly, the TIB ligand is not three coordinated, as commonly observed, but only bridges two Cd(II) ions with two nitrogen atoms, while the third nitrogen atom remains uncoordinated and exhibits substitutional disorder with the neighbouring C18 atom. Such a connection results in a wave-like Cd–TIB chain with a deeper "wave" than that of Cd–BPDP (ESI,† Fig. S6). The cross interconnection of these two kinds of wave-like chains leads to a 3D framework with 1D nanochannels of dimensions 9.7 × 13.0 $Å^2$ along the *b*-axis (Fig. 8a). The ester groups of the BPDP ligand point toward the channels. The effective free volume is about 18.2%, as calculated by PLATON.[20] As described above, the Cd(II) ion can be regarded as a four-connected node, while both the BPDP and TIB ligands can be simplified as lines, thus the whole network can be extended to a 4-connected $CdSO_4$ net with the Schläfli symbol ($6^5{\cdot}8$) (Fig. 8b).[21]

Structure differences in all compounds caused by N-donor ligands

The phosphonate monoester ligand in this work only bridges M(II) cations to form M–BPDP chains because coordination between M(II) and the oxygen atoms from the P═O bonds does not occur. The auxiliary N-donor ligands play a crucial role in both the structural diversity and the dimensionality

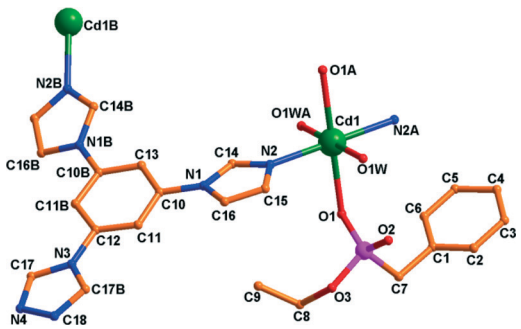

Fig. 7 Coordination environment of the cadmium(II) center and the binding fashion of the BPDP and TIB ligands in compound **4**. Symmetry code: A 0.5 − *x*, 0.5 − *y*, 1 − *z*; B 1 − *x*, *y*, 1.5 − *z*. The atoms marked as N4 and C18 exhibit substitutional disorder.

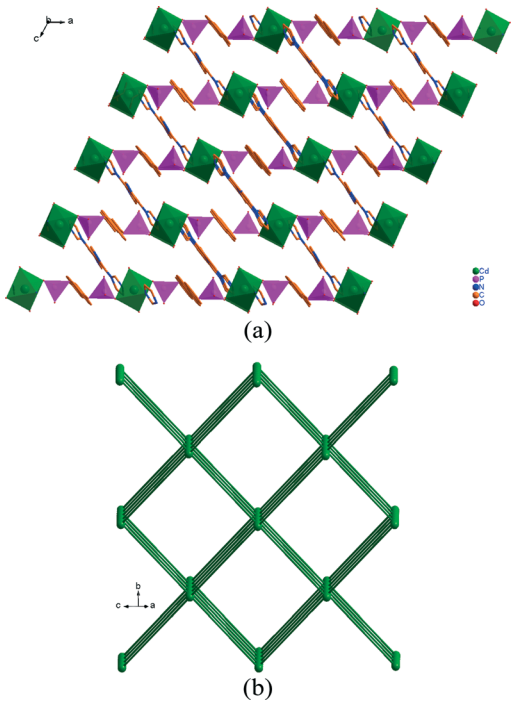

Fig. 8 (a) View of the 3D network in compound **4** with 1D nanochannels along the *b*-axis. The CdO_4N_2 and PCO_3 polyhedra are shown in green and purple, respectively. The ester groups in the BPDP ligand that point toward the channels and the guest molecules located at the channels are omitted for clarity. (b) Topological view of the 4-connected $CdSO_4$ net, in which the Cd(II) ions are simplified as 4-connected nodes, while both ligands are shown as lines.

variation of the resultant MOFs. In compound **1**, BIM ligands act as bridges to connect Cd(II) ions to form chains, and the Cd–BPDP and Cd–BIM chains interlock in parallel to afford 1D double-chains, which are further assembled into a compact three-dimensional structure *via* van der Waals forces. For compound **2**, the BIM ligands connect Cd(II) ions to give 1D nanoribbons, which are interconnected with Cd–BPDP chains from different directions to construct a thick 2D double-layered structure. In compound **3**, the TIB ligands behave as 3-connected nodes and connect Co(II) ions to result in a graphene-like 2D layer, in which two Co(II) cations in the same "6-membered ring" are further reinforced by a BPDP bridge, giving rise to a (3,5)-connected layer structure. The TIB ligands in the isomorphous compounds **4–6** only bridge two M(II) ions to form a wave-like chain, because one of the three N donors in TIB remains uncoordinated. The cross interconnection of M–BPDP and M–TIB chains leads to a 4-connected 3D network with $CdSO_4$ topology and 1D nanochannels along the *b*-axis.

Moisture stability

In previous reports, MOFs have shown powerful abilities to tune their composition, structure, pore size/environment, and structure-related properties. However, stability, especially moisture/chemical stability, has been recognized as a very challenging issue for the practical applications of MOFs as functional materials. So far, most MOFs are sensitive to moisture, which could be one of the key limitations to meeting the requirements of various applications. The classical Zn_4O-based carboxylate MOFs (such as MOF-5, MOF-177, the IRMOF series or the UMCM series)[6,22] and many Cd-based carboxylate MOFs[4b,18] are generally moisture- or even air-sensitive, because the bonds between the Zn(II)/Cd(II) ions and the carboxylic acid oxygen atoms are not robust enough to tolerate attack by water molecules. The carboxylate groups can be replaced by phosphonate monoester ligands, $[RPO_2(OCH_2CH_3)]^-$, which can provide two oxygen donor atoms and a monoanionic charge, similar to carboxylates. The additional ethyl groups in the phosphonate monoester might act as a steric shield to protect the M–O bonds and thus improve the moisture stability of the resultant MOFs. As expected, the obtained compounds exhibit enhanced moisture stability. As shown in Fig. 9, the powder X-ray diffraction (XRD) patterns indicate that the MOFs have very good stability, and that their frameworks are retained well upon exposure to moisture with 30–50% humidity for a couple of days. These results elegantly demonstrate that MOFs based on phosphonate monoesters have superior moisture stabilities.

Thermogravimetric analysis

Almost all of the compounds exhibit two main stages of weight loss, in which the first stage corresponds to removal of isolated or/and coordinated water molecules, and the second weight loss corresponds to framework collapse, as shown in Fig. 10. Decomposition of the compounds during thermogravimetric (TG) analysis is not completed until 700 °C, which has been previously reported for metal phosphonate compounds.[23] The TG curve of compound **1** shows that the first stage starts at 100 °C and is completed at 165 °C, which corresponds to the release of two coordinated water molecules. The observed weight loss is exactly the same as the calculated value (5.2%). After a short plateau, combustion of the organic ligands starts at 184 °C. The TG curve of compound **3** indicates that it starts to lose weight very slowly from room temperature to ~100 °C, then rapidly loses weight until 168 °C, releasing its isolated and coordinated water molecules. The observed weight loss of 10.5% is lower than the calculated value (16.4%). It should be mentioned that such deviation is common for MOFs and is usually caused by the spontaneous evaporation of uncoordinated solvent during the sample handling process prior to the TG experiment, especially when the compound contains a large number of lattice solvent molecules. After a long plateau, the organic ligands start to combust at 275 °C, and the weight loss does not end until 700 °C. Given the structure similarity, the weight loss curves of compounds **4** and **6** are comparable. Compound **4** slowly loses weight from room temperature, and then rapidly loses weight between 50 and 120 °C, corresponding to the release of isolated solvent molecules. Similarly, the weight loss of compound **6** between

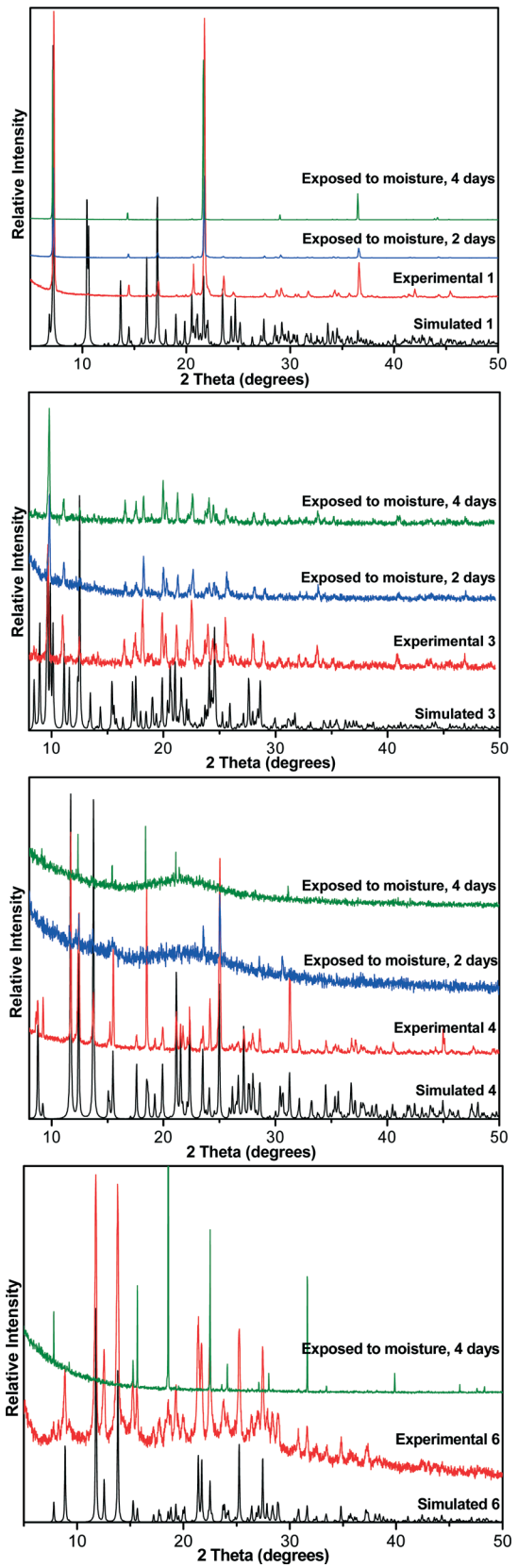

Fig. 9 Simulated and experimental powder XRD profiles of **1**, **3**, **4** and **6**, and their powder XRD patterns upon exposure to moisture (40–50% humidity for **1** and **4**; 30% humidity for **3** and **6**) for 2 and 4 days.

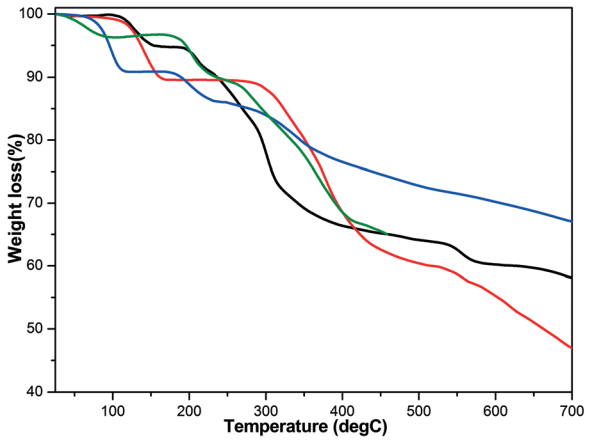

Fig. 10 TG curves for compounds **1** (black), **3** (red), **4** (blue) and **6** (green).

room temperature and 100 °C should be caused by the removal of uncoordinated water molecules. In this step, the observed weight losses are 9.1% and 3.7% for compounds **4** and **6**, respectively. Both values are lower than the calculated ones, possibly caused by the spontaneous loss in air of partially isolated H_2O molecules for both compounds before the TG experiment. Compounds **4** and **6** both exhibit plateaus before the second weight loss starts at 170 °C, which should be initiated by removal of coordinated water molecules, and further triggers combustion of the organic ligands and framework collapse.

Gas adsorption properties

The gas sorption of MOFs based on phosphonate ligands is seldom studied because the common phosphonic acid provides three oxygen atoms that can coordinate to metal cations, and the resultant metal phosphonates are usually nonporous or have tiny pores. In previous reports, phosphonate monoesters as carboxylate linkers gave MOFs with suitable pore sizes and certain gas sorption capabilities.[12c–e] In this work, the phosphonate monoester behaves as a bridge to connect metal ions to form porous 3D frameworks with moderate 1D nanochannels in compounds **4**–**6**. Upon removal of solvent molecules by evacuation, CO_2 adsorption studies at 195 K revealed gas sorptions of approximately 30 $cm^3\ g^{-1}$ and 40 $cm^3\ g^{-1}$ for compounds **4** and **6**, respectively. The results reveal the presence of permanent porosity, and correspond to Langmuir surface areas of 16 and 70 $m^2\ g^{-1}$ for compounds **4** and **6**, respectively.

Fluorescence properties

The solid-state luminescence properties of compounds **1**, **4** and **6**, as well as the BPDP, BIM and TIB ligands were investigated at room temperature (Fig. 11 and S10†). The BPDP and BIM ligands exhibit fluorescence emission bands at λ_{max} = 340 and 347 nm, respectively, under excitation at 278 nm. Upon combination of the BPDP and BIM ligands with Cd(II) ions, compound **1** displays a strong fluorescence emission

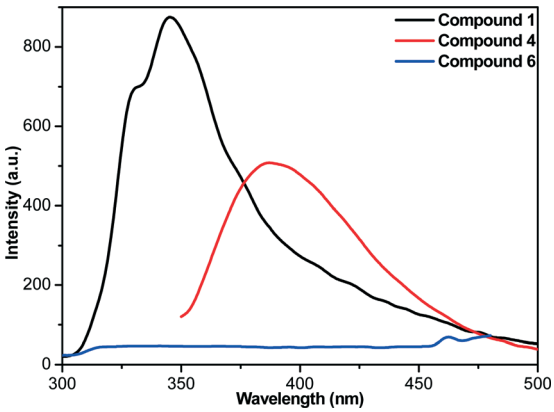

Fig. 11 Solid-state emission spectra of compounds **1** (black, λ_{ex} = 278 nm), **4** (red, λ_{ex} = 330 nm), and **6** (blue, λ_{ex} = 253 nm) at room temperature.

band at λ_{max} = 346 nm (λ_{ex} = 278 nm), which is very close to the ligand emission bands, and could thus originate from intraligand transitions. The TIB ligand displays weak and broad fluorescence emission ranging from 378 to 392 nm upon excitation at 330 nm. Under the same excitation, compound **4** shows strong solid-state fluorescence at λ_{max} = 387 nm, which could also be assigned to intraligand transitions. The very weak fluorescence intensity of compound **6** could be due to the quenching effect of the Cu(II) ions.

Conclusions

In conclusion, six MOFs based on a phosphonate monoester ligand with structure dimensionalities ranging from 1D to 3D have been synthesized. The auxiliary N-donor ligands, BIM and TIB, have shown subtle effects on the structural diversity and dimensionality variation of the resultant MOFs. More importantly, with the steric protection of the ethyl groups (in the BPDP ligands) as a shield for the hydrolytically vulnerable M–O bonds, the obtained MOFs have considerable stability and remain stable upon exposure to moisture with 30–50% humidity for 2–4 days, which would facilitate their functional applications. The MOFs with 3D porous networks have exhibited CO_2 gas sorption properties, which revealed their permanent porosity. The Cd-based MOFs have also shown strong fluorescence emission assigned to intraligand transitions. The successful preparation of these MOFs based on an elongated phosphonate bis(monoester) ligand provides a valuable approach for the construction of MOFs with tuneable structures and improved moisture stabilities. The exploration of phosphonate monoester moieties with other ligand skeletons for MOF synthesis is currently underway in our laboratory.

Acknowledgements

This work was supported by the National Natural Science Foundation of China (21361002, Z.Y.D.; 21371162 and 51301159, H.L.J.), and the Young Scientists Training Program of Jiangxi Province (20122BCB23020, Z.Y.D.). H.L.J. also thanks the Research Fund for the Doctoral Program of Higher Education of China (20133402120020), the Scientific Research Foundation for the Returned Overseas Chinese Scholars, the State Education Ministry and the Fundamental Research Funds for the Central Universities (WK2060190026).

Notes and references

1 (*a*) S. Horike, S. Shimomura and S. Kitagawa, *Nat. Chem.*, 2009, **1**, 695; (*b*) J. R. Long and O. M. Yaghi, *Chem. Soc. Rev.*, 2009, **38**, 1213; (*c*) Z. Wang and S. M. Cohen, *Chem. Soc. Rev.*, 2009, **38**, 1315; (*d*) J. J. Perry IV, J. A. Perman and M. J. Zaworotko, *Chem. Soc. Rev.*, 2009, **38**, 1400; (*e*) H.-C. Zhou, J. R. Long and O. M. Yaghi, *Chem. Rev.*, 2012, **112**, 673.

2 (*a*) H. Wu, W. Zhou and T. Yildirim, *J. Am. Chem. Soc.*, 2009, **131**, 4995; (*b*) R. Vaidhyanathan, S. S. Iremonger, G. K. H. Shimizu, P. G. Boyd, S. Alavi and T. K. Woo, *Science*, 2010, **330**, 650; (*c*) K. Sumida, D. L. Rogow, J. A. Mason, T. M. McDonald, E. D. Bloch, Z. R. Herm, T.-H. Bae and J. R. Long, *Chem. Rev.*, 2012, **112**, 724; (*d*) M. P. Suh, H. J. Park, T. K. Prasad and D.-W. Lim, *Chem. Rev.*, 2012, **112**, 782; (*e*) J.-R. Li, J. Sculley and H.-C. Zhou, *Chem. Rev.*, 2012, **112**, 869.

3 (*a*) J. S. Seo, D. Whang, H. Lee, S. I. Jun, J. Oh, Y. J. Jeon and K. Kim, *Nature*, 2000, **404**, 982; (*b*) L. Ma, C. Abney and W. Lin, *Chem. Soc. Rev.*, 2009, **38**, 1248; (*c*) D. Farrusseng, S. Aguado and C. Pinel, *Angew. Chem., Int. Ed.*, 2009, **48**, 7502; (*d*) A. Corma, H. García and F. X. Llabrés i Xamena, *Chem. Rev.*, 2010, **110**, 4606; (*e*) H.-L. Jiang and Q. Xu, *Chem. Commun.*, 2011, **47**, 3351; (*f*) Z. Zhang, L. Zhang, L. Wojtas, M. Eddaoudi and M. J. Zaworotko, *J. Am. Chem. Soc.*, 2012, **134**, 928.

4 (*a*) B. Chen, S. Xiang and G. Qian, *Acc. Chem. Res.*, 2010, **43**, 1115; (*b*) H.-L. Jiang, Y. Tatsu, Z.-H. Lu and Q. Xu, *J. Am. Chem. Soc.*, 2010, **132**, 5586; (*c*) Y. Takashima, V. Martinez, S. Furukawa, M. Kondo, S. Shimomura, H. Uehara, M. Nakahama, K. Sugimoto and S. Kitagawa, *Nat. Commun.*, 2011, **2**, 168; (*d*) L. E. Kreno, K. Leong, O. K. Farha, M. Allendorf, R. P. Van Duyne and J. T. Hupp, *Chem. Rev.*, 2012, **112**, 1105.

5 (*a*) J. An, S. J. Geib and N. L. Rosi, *J. Am. Chem. Soc.*, 2009, **131**, 8376; (*b*) J. D. Rocca, D. Liu and W. Lin, *Acc. Chem. Res.*, 2011, **44**, 957; (*c*) P. Horcajada, R. Gref, T. Baati, P. K. Allan, G. Maurin, P. Couvreur, G. Férey, R. E. Morris and C. Serre, *Chem. Rev.*, 2012, **112**, 1232.

6 (*a*) H. Li, M. Eddaoudi, M. O'Keeffe and O. M. Yaghi, *Nature*, 1999, **402**, 276; (*b*) J. A. Greathouse and M. D. Allendorf, *J. Am. Chem. Soc.*, 2006, **128**, 10678; (*c*) S. S. Kaye, A. Dailly, O. M. Yaghi and J. R. Long, *J. Am. Chem. Soc.*, 2007, **129**, 14176.

7 (*a*) K. S. Park, Z. Ni, A. P. Côté, J. Y. Choi, R. Huang, F. J. Uribe-Romo, H. K. Chae, M. O'Keeffe and O. M. Yaghi, *Proc. Natl. Acad. Sci. U. S. A.*, 2006, **103**, 10186; (*b*) X. C. Huang, Y. Y. Lin, J. P. Zhang and X. M. Chen, *Angew.*

Chem., Int. Ed., 2006, **45**, 1557; (*c*) G. Férey, C. Mellot-Draznieks, C. Serre, F. Millange, J. Dutour, S. Surblé and I. Margiolaki, *Science*, 2005, **309**, 2040; (*d*) G. Férey, C. Serre, C. Mellot-Draznieks, F. Millange, S. Surblé, J. Dutour and I. Margiolaki, *Angew. Chem., Int. Ed.*, 2004, **43**, 6296.

8 (*a*) J. H. Cavka, S. Jakobsen, U. Olsbye, N. Guillou, C. Lamberti, S. Bordiga and K. P. Lillerud, *J. Am. Chem. Soc.*, 2008, **130**, 13850; (*b*) V. Colombo, S. Galli, H. J. Choi, G. D. Han, A. Maspero, G. Palmisano, N. Masciocchi and J. R. Long, *Chem. Sci.*, 2011, **2**, 1311.

9 (*a*) H.-L. Jiang, D. Feng, T.-F. Liu, J.-R. Li and H.-C. Zhou, *J. Am. Chem. Soc.*, 2012, **134**, 14690; (*b*) D. Feng, Z.-Y. Gu, J.-R. Li, H.-L. Jiang, Z. Wei and H.-C. Zhou, *Angew. Chem., Int. Ed.*, 2012, **51**, 10307; (*c*) H.-L. Jiang, D. Feng, K. Wang, Z.-Y. Gu, Z. Wei, Y.-P. Chen and H.-C. Zhou, *J. Am. Chem. Soc.*, 2013, **135**, 13934; (*d*) D. Feng, W.-C. Chung, Z. Wei, Z.-Y. Gu, H.-L. Jiang, D. J. Darensbourg and H.-C. Zhou, *J. Am. Chem. Soc.*, 2013, **135**, 17105; (*e*) D. Feng, H.-L. Jiang, Y.-P. Chen, Z.-Y. Gu, Z. Wei and H.-C. Zhou, *Inorg. Chem.*, 2013, **52**, 12661.

10 (*a*) J. H. Cavka, S. Jakobsen, U. Olsbye, N. Guillou, C. Lamberti, S. Bordiga and K. P. Lillerud, *J. Am. Chem. Soc.*, 2008, **130**, 13850; (*b*) M. Kandiah, M. H. Nilsen, S. Usseglio, S. Jakobsen, U. Olsbye, M. Tilset, C. Larabi, E. A. Quadrelli, F. Bonino and K. P. Lillerud, *Chem. Mater.*, 2010, **22**, 6632; (*c*) A. Schaate, P. Roy, A. Godt, J. Lippke, F. Waltz, M. Wiebcke and P. Behrens, *Chem. - Eur. J.*, 2011, **17**, 6643; (*d*) A. Schaate, P. Roy, T. Preuße, S. J. Lohmeier, A. Godt and P. Behrens, *Chem. - Eur. J.*, 2011, **17**, 9320; (*e*) W. Morris, B. Volosskiy, S. Demir, F. Gándara, P. L. McGrier, H. Furukawa, D. Cascio, J. F. Stoddart and O. M. Yaghi, *Inorg. Chem.*, 2012, **51**, 6443; (*f*) V. Bon, V. Senkovskyy, I. Senkovska and S. Kaskel, *Chem. Commun.*, 2012, **48**, 8407; (*g*) V. Guillerm, F. Ragon, M. Dan-Hardi, T. Devic, M. Vishnuvarthan, B. Campo, A. Vimont, G. Clet, Q. Yang, G. Maurin, G. Férey, A. Vittadini, S. Gross and C. Serre, *Angew. Chem., Int. Ed.*, 2012, **51**, 9267.

11 (*a*) A. Clearfield, Metal phosphonate chemistry, in *Progress in Inorganic Chemistry*, ed. K. D. Karlin, Wiley, New York, 1998, vol. 47, p. 371; (*b*) K. Maeda, *Microporous Mesoporous Mater.*, 2004, **73**, 47; (*c*) J.-G. Mao, *Coord. Chem. Rev.*, 2007, **251**, 1493; (*d*) G. K. H. Shimizu, R. Vaidhyanathan and J. M. Taylor, *Chem. Soc. Rev.*, 2009, **38**, 1430; (*e*) K. J. Gagnon, H. P. Perry and A. Clearfield, *Chem. Rev.*, 2012, **112**, 1034.

12 (*a*) O. R. Evans, D. R. Manke and W. Lin, *Chem. Mater.*, 2002, **14**, 3866; (*b*) M. Kontturi, E. Laurila, R. Mattsson, S. Peräniemi, J. J. Vepsäläinen and M. Ahlgrén, *Inorg. Chem.*, 2005, **44**, 2400; (*c*) S. S. Iremonger, J. Liang, R. Vaidhyanathan and G. K. H. Shimizu, *Chem. Commun.*, 2011, **47**, 4430; (*d*) S. S. Iremonger, J. Liang, R. Vaidyanathan, I. Martens, G. K. H. Shimizu, T. D. Daff, M. Z. Aghaji, S. Yeganegi and T. K. Woo, *J. Am. Chem. Soc.*, 2011, **133**, 20048; (*e*) J. M. Taylor, R. Vaidhyanathan, S. S. Iremonger and G. K. H. Shimizu, *J. Am. Chem. Soc.*, 2012, **134**, 14338; (*f*) T. Yamada and H. Kitagawa, *CrystEngComm*, 2012, **14**, 4148.

13 J. G. Nguyen and S. M. Cohen, *J. Am. Chem. Soc.*, 2010, **132**, 4560.

14 (*a*) C. R. Mayer, M. Hervé, H. Lavanant, J.-C. Blais and F. Sécheresse, *Eur. J. Inorg. Chem.*, 2004, 973; (*b*) J. Cai, T. Zhao, G. An, B. Zhou and Q. Hu, *Huaxue Yu Shengwu Gongcheng*, 2009, **26**, 22; (*c*) A. Rit, T. Pape, A. Hepp and F. E. Hahn, *Organometallics*, 2011, **30**, 334.

15 *APEX2, SADABS and SAINT*, Bruker AXS Inc., Madison, Wisconsin, USA, 2008.

16 (*a*) G. M. Sheldrick, *SHELXS-97, Program for X-ray Crystal Structure Solution*, University of Göttingen, Germany, 1997; (*b*) G. M. Sheldrick, *SHELXL-97, Program for X-ray Crystal Structure Refinement*, University of Göttingen, Germany, 1997.

17 A. L. Spek, *Acta Crystallogr., Sect. D: Biol. Crystallogr.*, 2009, **65**, 148.

18 (*a*) H. Yang, F. Wang, Y.-X. Tan, T.-H. Li and J. Zhang, *Chem. - Asian J.*, 2012, **7**, 1069; (*b*) J. Guo, D. Sun, L. Zhang, Q. Yang, X. Zhao and D. Sun, *Cryst. Growth Des.*, 2012, **12**, 5649.

19 (*a*) L. Chen, G.-J. Xu, K.-Z. Shao, Y.-H. Zhao, G.-S. Yang, Y.-Q. Lan, X.-L. Wang, H.-B. Xu and Z.-M. Su, *CrystEngComm*, 2010, **12**, 2157; (*b*) W. Yang, M. Guo, F.-Y. Yi and Z.-M. Sun, *Cryst. Growth Des.*, 2012, **12**, 5529; (*c*) T. Panda, K. M. Gupta, J. Jiang and R. Banerjee, *CrystEngComm*, 2014, **16**, 4677.

20 A. L. Spek, *J. Appl. Crystallogr.*, 2003, **36**, 7.

21 (*a*) A. F. Wells, *Three-Dimensional Nets and Polyhedra*, Wiley, New York, 1977; (*b*) S. R. Batten and R. Robson, *Angew. Chem., Int. Ed.*, 1998, **37**, 1460; (*c*) N. W. Ockwig, O. Delgado-Fridedrichs, M. O'Keeffe and O. M. Yaghi, *Acc. Chem. Res.*, 2005, **38**, 176.

22 (*a*) M. Eddaoudi, J. Kim, N. Rosi, D. Vodak, J. Wachter, M. O'Keeffe and O. M. Yaghi, *Science*, 2002, **295**, 469; (*b*) H. K. Chae, D. Y. Siberio-Pérez, J. Kim, Y. Go, M. Eddaoudi, A. J. Matzger, M. O'Keeffe and O. M. Yaghi, *Nature*, 2004, **427**, 523; (*c*) K. Koh, A. G. Wong-Foy and A. J. Matzger, *Angew. Chem., Int. Ed.*, 2008, **47**, 677; (*d*) K. Koh, A. G. Wong-Foy and A. J. Matzger, *J. Am. Chem. Soc.*, 2009, **131**, 4184.

23 Z.-Y. Du, X.-L. Li, Q.-Y. Liu and J.-G. Mao, *Cryst. Growth Des.*, 2007, **7**, 1501.

